Evaluation of 4-D Reaction Integrals in the Method of Moments: Coplanar Element Case

Evaluation of 4-D Reaction Integrals in the Method of Moments: Co-planar Element Case

D. R. Wilton, *Life Fellow, IEEE*, F. Vipiana, *Senior Member, IEEE*,
W. A. Johnson, *Senior Member, IEEE*

***Abstract*—Recently the benefits of simultaneously treating source and testing integrals in the numerical evaluation of 4-D reaction integrals have been reported. The reported schemes usually first transform the reaction integral to parametric coordinates, and some combination of radial, angular, and/or line segment integrals is then used to treat coincident, edge-adjacent, or vertex-adjacent triangular source and test element pairs. However advantages of the reported approaches are tempered by their lack of generality and severely degraded performance on poorly-shaped elements, the latter caused primarily by the parametric transformations' severe distortion of the kernel's circularly concentric level contours.**

Here, for coplanar element pairs and kernels with $1/R$ singularities, we apply the surface divergence theorem twice to obtain a novel formula for 4-D reaction integrals, generalizing earlier schemes while retaining their benefits and without distorting the original configuration space. Numerical results illustrate the method's efficiency, which is improved by employing appropriate transformations to further smooth the resulting integrands and hence accelerate their convergence. The reaction integral formula can be extended to non-coplanar elements.

***Index Terms*—integral equations, moment methods, numerical analysis, singular integrals.**

I. Introduction

The numerical integration of double surface integrals is fundamental to moment method solutions of surface integral equations (SIEs). SIEs have emerged as the dominant technology for modeling large and complex structures such as naval, aerospace, satellite, and antenna structures with unknowns confined to body surfaces. Even more critical, however, are periodic and/or layered media problems, where the Green's function calculation costs per sample point are often hundreds of times that for homogeneous media, and efficient methods with good accuracy are essential.

Recently element mappings and radial integrations were used to develop powerful numerical methods for handling general kernels on both curved and flat triangular source and test elements [1]. The development of related analytical, numerical, and hybrid analytic-numerical approaches to this 4-D integration problem can be traced in [2][3][4][5]. They address the general problem of handling the 4-D integration of singular and near-singular reaction integrals of the method of moments (MoM) over surface source and test element pairs. Ad hoc methods are generally used, however, that treat only self-interacting, edge-adjacent, or vertex-adjacent elements, and are generally limited to well-shaped (i.e., nearly equilateral) triangular element pairs.

In this paper, we employ the surface divergence theorem twice to evaluate the two surface integrals involved for coplanar elements and kernels with $1/R$ singularities, where $R=|\mathbf{r}-\mathbf{r}'|$ and $\mathbf{r}$ and $\mathbf{r}'$ are observation and source points, respectively. The surface divergence theorem has been used, for example in [6], to handle singular *source* integrals, but its subsequent application to *testing* integrals has been essentially limited to ad hoc analytical and semi-analytical evaluations for (4-D) reaction integrals involving linear basis and test functions with static kernels and on planar domains [7][8]. Here, we use the surface divergence theorem for both source and testing integrals, generalizing the approach of [8] while retaining the beneficial features of [1] without some of its restrictions. In this paper, for simplicity, we restrict consideration to co-planar elements and homogeneous media potential kernels. This restricted case does, however, handle the moment method's critical "self"-terms" for planar elements. (We note that kernels of the form $\nabla(1/R)$ are also of considerable interest, but in the coplanar case the principal value contribution from the source integral reduces to a delta-function, and the resulting test integration reduces simply to an analytical evaluation of the inner product between basis and testing functions. A numerical treatment for this case is therefore relevant only for non-coplanar elements.)

Specifically, we apply the surface divergence theorem to the source and test integrals, obtaining a novel, general expression for the reaction between coplanar elements with arbitrary kernels, bases, and testing functions. The result is particularly suited, however, for kernels bounded by singularities of order $1/R$. The resulting representation has

Manuscript submitted for review on XXX

This work was supported in part by the Microwave Imaging for Combined Early Diagnostics of Breast Cancer (MICENEA) FIRB project.

D. R. Wilton is with the Department of Electrical and Computer Engineering, University of Houston, Houston, TX 77204-4005 USA (e-mail: wilton@uh.edu).

F. Vipiana is with the Department of Electronics and Telecommunications, Politecnico di Torino, 10129 Torino, Italy (email: francesca.vipiana@polito.it).

W. A. Johnson is with the Department of Mathematics, New Mexico Institute of Mining and Technology, Socorro, NM 87801 USA (email: William.Johnson@nmt.edu).

features in common with those of [1], with two inner radial integrals and two outer integrals over source and test element boundaries. But the integral domains are not parametrically mapped, thus freeing the scheme from restrictions to well-shaped coincident or adjacent elements.

Though the derived general expression automatically regularizes kernels with singularities of order $1/R$ and hence can be applied directly, its efficiency can be significantly improved by using a static kernel with constant basis and testing functions as a model integrand to develop transformations for the contour integrals that provide an *exact* result for such kernels. Further, the transforms significantly accelerate the numerical evaluation for dynamic kernels and for linear basis and testing functions, and for even more general integrands of kernels with singularities bounded by 1/*R*. We demonstrate that the new representation is robust, and can be used with straightforward Gauss-Legendre quadrature rules for reasonable accuracy, or double exponential quadrature rules [9] for essentially arbitrary precision. Accurate evaluation of these interactions often mitigates problems due to the error amplification in certain inherently ill-conditioned integral equations such as the electric field integral equation (EFIE). Such difficulties appear not only with high density, distorted, and non-uniform meshes, but also near internal resonances, and due to inability to maintain linear independence as with increasingly higher order bases. We usually associate such problems with Green's functions for homogeneous media, but for problems in which Green's function evaluation costs are typically hundreds of times greater (e.g. layered and/or periodic media), one often faces a different problem: significantly reducing the number of kernel evaluations to gain speed. In this case, one frequently settles for slightly reduced accuracy—and perhaps a moderately higher overhead cost per evaluation—in order to substantially reduce the number of Green's function evaluations.

For (vector) linear basis and testing functions and homogeneous medium kernels, we show that the radial integrals can be evaluated in closed form. Alternatively, or for kernels merely *bounded* by such kernels, such as layered media or periodic Green's function kernels, a purely numerical approach to radial integration may be necessary. In this case a scheme is offered that optimizes the radial quadrature rule choice to obtain a specified accuracy.

The paper is organized as follows. In Sect. II, the general expression for 4D reaction integrals between a pair of coplanar elements is derived. Sect. III is devoted to the evaluation of the radial integrals, while Sect. IV deals with variable transformations applied to accelerate the numerical evaluation of the contour integrals. In Sect. V several numerical results are presented, and Sect. VI contains conclusions and discusses possible extensions to the approach. Preliminary results for the proposed approach were presented in [10].

II. Reaction Integral for a Coplanar Element Pair

Our interest is in performing accurate and efficient integration of double surface integrals of the form

$$\int_S \int_{S'} F(\mathbf{r},\mathbf{r}')\, dS'\, dS, \tag{1}$$

where $F(\mathbf{r},\mathbf{r}')$ is a scalar function of a source point $\mathbf{r}'$ and observation point $\mathbf{r}$. For simplicity, we treat here only the coplanar case. This, in effect, reduces $\mathbf{r}$ and $\mathbf{r}'$ to vectors in the plane of S and S'. Usually $F(\mathbf{r},\mathbf{r}')$ has a singularity of order $\mathcal{O}\left(1/|\mathbf{r}-\mathbf{r}'|\right)$, and typically takes the form

$$F(\mathbf{r},\mathbf{r}') = t(\mathbf{r})G(\mathbf{r},\mathbf{r}')b(\mathbf{r}'), \tag{2}$$

where $b(\mathbf{r}')$ and $t(\mathbf{r})$ are basis and testing functions and $G(\mathbf{r},\mathbf{r}')$ is a Green's function with singularity at $\mathbf{r}=\mathbf{r}'$. (For vector bases or dyadic kernels, terms in (2) are vector or dyadic *components*, respectively.) The usual approach for evaluating (1) is to first carefully evaluate the inner (singular) integral over S', then, assuming the resulting integral is non-singular, evaluate the outer integral over S using straightforward Gauss quadrature [11][12][13]. Not only does this approach place undue burden on evaluation of the source integral, but the assumption of smoothness of the test integral integrand is actually invalid when boundaries of S and S' are in contact [1][14].

A. Source Integration Using the Divergence Theorem

To evaluate (1), we first consider applying the divergence theorem to evaluate the innermost surface integral on primed coordinates. The idea is to find a vector function $\mathbf{H}(\mathbf{r},\mathbf{r}')$ such that $\nabla'\cdot\mathbf{H} = F(\mathbf{r},\mathbf{r}')$, and reduce the surface integral to a line integral via the surface divergence theorem,

$$\int_{S'} F(\mathbf{r},\mathbf{r}')\, dS' = \oint_{C'} \mathbf{H}(\mathbf{r},\mathbf{r}'_{C'})\cdot\hat{\mathbf{u}}'\, dC', \tag{3}$$

where C' is the boundary of S', $\mathbf{r}'_{C'}$ is a point on C', and $\hat{\mathbf{u}}'$ is a unit vector along the outward normal to the boundary of S' and in the plane of S'. To determine the vector $\mathbf{H}(\mathbf{r},\mathbf{r}')$, assume it has only a single, radial component with respect to a fixed value of $\mathbf{r}$, i.e., $\mathbf{H}(\mathbf{r},\mathbf{r}') = \hat{\mathbf{D}}' H(\mathbf{r},\mathbf{r}')$, where $\hat{\mathbf{D}}' = (\mathbf{r}'-\mathbf{r})/D'$ is a radial unit vector and $D' = |\mathbf{r}'-\mathbf{r}|$ is a radial distance between $\mathbf{r}$ and the source point in the plane of S and S'. Then for fixed $\mathbf{r}$ the surface divergence is

$$\nabla'\cdot\mathbf{H} = \frac{1}{D'}\frac{d}{dD'}\left(D'H\right) = F(\mathbf{r},\mathbf{r}+D'\hat{\mathbf{D}}'). \tag{4}$$

Integration of (4) with respect to D' over the interval $0 \le D' \le D = |\mathbf{r}-\mathbf{r}'_{C'}|$ thus yields

$$\mathbf{H}(\mathbf{r},\mathbf{r}'_{C'}) = \frac{\hat{\mathbf{D}}'}{D}\int_0^D F(\mathbf{r},\mathbf{r}+D'\hat{\mathbf{D}}')\, D'dD'. \tag{5}$$

Combining (3) and (5), we obtain

$$\int_{S'} F(\mathbf{r},\mathbf{r}')\, dS' = \oint_{C'} \hat{\mathbf{u}}'\cdot\left(\frac{\hat{\mathbf{D}}'}{D}\int_0^D F(\mathbf{r},\mathbf{r}')\, D'dD'\right) dC', \tag{6}$$

where $\mathbf{r}' = \mathbf{r}+D'\hat{\mathbf{D}}'$. Equation (6) is easily generalized to vector or dyadic integrands by applying it component-wise,

yielding

$$\int_{S'} \mathcal{F}(\mathbf{r},\mathbf{r}')\,dS' = \oint_{C'} \hat{\mathbf{u}}' \cdot \left(\frac{\hat{\mathbf{D}}'}{D} \int_0^D \mathcal{F}(\mathbf{r},\mathbf{r}')\,D'dD' \right) dC', \qquad (7)$$

where $\mathcal{F}(\mathbf{r},\mathbf{r}')$ may be either a scalar, vector, or dyadic quantity. Results (6) and (7) are not novel; indeed they may be considered as generalizations of the fundamental theorem of calculus to two dimensions [15].

We also note that the contour integral of (6) may also be interpreted as integration in polar coordinates. For a point $\mathbf{r}$ outside the source contour C', Figure 1 shows contributions to the integral (6) from a region of angular width $d\phi'$.

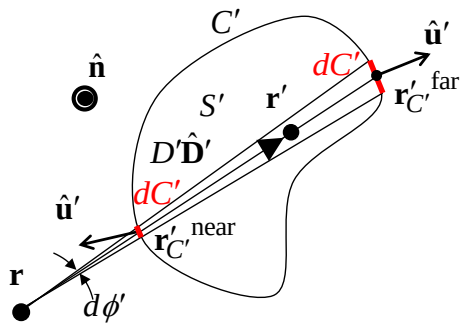

Figure 1. Radial path contributions to integral (6).

Noting that

$$d\phi' = \frac{\hat{\mathbf{D}}' \cdot \hat{\mathbf{u}}' dC'}{D}, \qquad (8)$$

where D is defined following (6), (6) can be rewritten as

$$\begin{aligned} \int_{S'} F(\mathbf{r},\mathbf{r}')\,dS' &= \int_{\phi(C')} \int_0^D F(\mathbf{r},\mathbf{r}')D'dD'\,d\phi' \\ &= \int_{\phi(C'^{\text{far}})} \int_{D(\mathbf{r}'^{\text{near}}_{C'})}^{D(\mathbf{r}'^{\text{far}}_{C'})} F(\mathbf{r},\mathbf{r}')D'dD'\,d\phi', \end{aligned} \qquad (9)$$

where the first line of (9) represents an integration in polar coordinates (D',ϕ') with an angular parameterization $\phi(C')$ of C', and the second line further accounts for the exact canceling of radial integral contributions along the ray $\hat{\mathbf{D}}'$ from equiangular differential segments lying outside C' (see Fig. 1). We emphasize that this pairing of canceling contour contributions conveniently restricts the integration to S', but is not generally necessary except possibly to reduce either cancellation error or the extent of the radial integration domain. It may also be desirable for multi-layer or periodic Green's functions where there is not only a possibility the Green's function is discontinuous (e.g. if $\mathbf{r}$ and S' are in different layers), but also a very high cost associated with evaluating it at non-contributing source points outside the source region.

B. *Test integration using the divergence theorem*

To evaluate the outer surface integral in the double surface integral (1), we integrate (6) over S, interchange order of integration and apply the divergence theorem again, this time using (7):

$$\begin{aligned} &\int_S \int_{S'} F(\mathbf{r},\mathbf{r}')\,dS'dS \\ &= \int_S \left[\oint_{C'} \hat{\mathbf{u}}' \cdot \left(\frac{\hat{\mathbf{D}}'}{D} \int_0^D F(\mathbf{r},\mathbf{r}')\,D'dD' \right) dC' \right] dS \\ &= \oint_{C'} \hat{\mathbf{u}}' \cdot \left[\int_S \left(\frac{\hat{\mathbf{D}}'}{D} \int_0^D F(\mathbf{r},\mathbf{r}')\,D'dD' \right) dS \right] dC' \\ &= \oint_C \oint_{C'} \frac{(\hat{\mathbf{u}} \cdot \hat{\mathbf{D}})(\hat{\mathbf{u}}' \cdot \hat{\mathbf{D}}')}{|\mathbf{r}_C - \mathbf{r}'_{C'}|} \left[\int_0^{|\mathbf{r}_C - \mathbf{r}'_{C'}|} \int_0^D F(\mathbf{r},\mathbf{r}')\,D'dD'\,dD \right] dC'dC, \end{aligned} \qquad (10)$$

where $\mathbf{r} = \mathbf{r}'_{C'} + D\hat{\mathbf{D}}$, and $\mathbf{r}_C\,(\mathbf{r}'_{C'})$ is a point on $C\,(C')$, as shown in Figure 2.

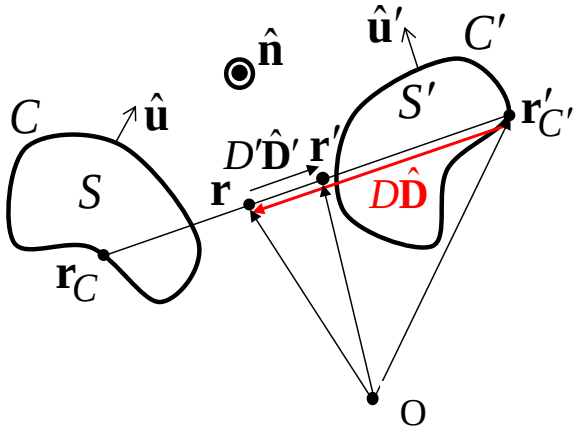

Figure 2. Two coplanar domains and geometrical definitions.

The inner double radial integral feature, which smoothes the integral and exactly cancels singularities of order $1/|\mathbf{r}-\mathbf{r}'| = 1/D'$ in the innermost (radial) integral of (10), is analogous to the representation of Polimeridis et al., [1]–[5] but is performed in the physical rather than in a mapped domain.

The general result (10) appears to be novel, though specialized versions of it have been used to analytically evaluate specific potential integrals [7][8]. Here, however, we focus on the numerical evaluation of the 4-D integral. We have noted that typical potential integrals involve a singularity of the form $F(\mathbf{r},\mathbf{r}') = \mathcal{O}\left(1/|\mathbf{r}-\mathbf{r}'|\right) = \mathcal{O}(1/D')$ which is exactly canceled by the first radial integral in (10).

For polygonal domains, such as the two coplanar triangles Figure 3, the remaining contour integrals may be implemented by successively integrating pairs of test and source domain edges making up the polygons' boundaries. Thus evaluating (10) reduces to evaluating integral contributions of the form

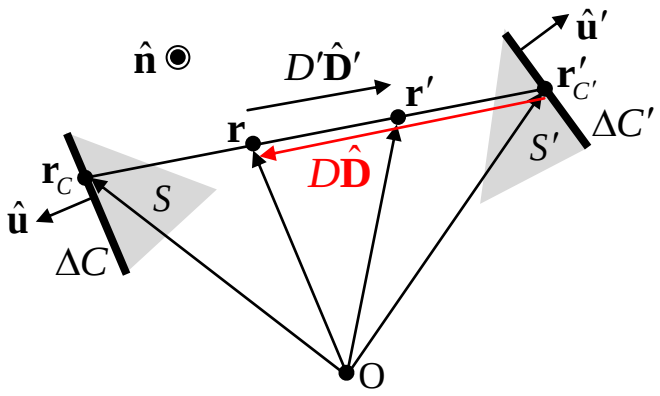

Figure 3. Definition of quantities needed in the computation of radial integrals associated with a pair of interacting edges $\Delta C'$ and ΔC for source triangle S' and test triangle S, respectively. The vector $\hat{\mathbf{n}}$ is the normal to the plane containing the two triangles. Outward normals to the test and source triangle edges are $\hat{\mathbf{u}}$ and $\hat{\mathbf{u}}'$, and the edges are oriented along the vectors $\hat{\boldsymbol{\ell}} = \hat{\mathbf{n}} \times \hat{\mathbf{u}}$ and $\hat{\boldsymbol{\ell}}' = \hat{\mathbf{n}} \times \hat{\mathbf{u}}'$, resp.

$$\int_{\rho_L}^{\rho_U} \int_{\rho_L'}^{\rho_U'} \left[\frac{(\hat{\mathbf{u}} \cdot \hat{\mathbf{D}})(\hat{\mathbf{u}}' \cdot \hat{\mathbf{D}}')}{|\mathbf{r}_C - \mathbf{r}_{C'}'|} \int_0^{|\mathbf{r}_C - \mathbf{r}_{C'}'|} \int_0^D F(\mathbf{r}, \mathbf{r}')\, D' dD' dD \right] d\rho' d\rho. \tag{11}$$

resulting from the interaction of line segment pairs ΔC and $\Delta C'$, parameterized by arc lengths ρ and ρ', respectively. Without loss of generality, in the following we assume edges ΔC and $\Delta C'$ belong to a pair of coplanar triangles, S and S', respectively, with each boundary edge directed in a right-handed sense with respect to its triangle's normal, $\hat{\mathbf{n}}$. Note that for a pair of collinear edges, both dot products and hence the corresponding edge-pair integral (11) vanish. For non-collinear edges, straightforward Gauss-Legendre quadrature of sufficiently high order can, in principle, furnish any desired level of accuracy; in practice, if one desires more than modest accuracy (say, 5 or more significant digits), increasing the quadrature order can quickly reach a point of diminishing returns. To counter this tendency, or to simply improve convergence, it is useful to transform the contour integrals (11) into faster converging forms, as discussed in Sect. IV.

III. Radial Integral Evaluation

For polynomial basis and testing functions and the homogeneous medium kernel, the radial integrals may be evaluated in closed form, and this is a particularly efficient approach. But for kernels associated with, for example, periodic or multilayered media Green's functions, this approach may not be practical and a purely numerical approach is preferred. For homogeneous kernels or those bounded by homogenous kernels, it is also possible to optimize the choice of quadrature rule. We examine these three possibilities in the following sections.

A. Analytical evaluation

For standard RWG bases and testing functions [16], the radial integrals for the vector potential become

$$\frac{1}{4\pi} \int_0^{|\mathbf{r}_C - \mathbf{r}_{C'}'|} \int_0^D \boldsymbol{\Lambda}_i^e(\mathbf{r}) \cdot \boldsymbol{\Lambda}_j^f(\mathbf{r}') \frac{e^{-jk|\mathbf{r}-\mathbf{r}'|}}{|\mathbf{r}-\mathbf{r}'|} D' dD' dD, \tag{12}$$

where the (unnormalized) testing function associated with the ith edge of element e and the source basis function associated with the jth edge of element f can be written, resp., as

$$\boldsymbol{\Lambda}_i^e(\mathbf{r}) = \mathbf{r} - \mathbf{r}_i^e = \mathbf{r}_{C'}' - \mathbf{r}_i^e + D\hat{\mathbf{D}}, \tag{13}$$

$$\boldsymbol{\Lambda}_j^f(\mathbf{r}') = \mathbf{r}' - \mathbf{r}_j^f = \mathbf{r}_{C'}' - \mathbf{r}_j^f + D\hat{\mathbf{D}} + D'\hat{\mathbf{D}}'. \tag{14}$$

In (13) and (14), $\mathbf{r}_i^e$ and $\mathbf{r}_j^f$, $i, j = 1,2,3$, are the vertices opposite the ith and jth test and source triangle edges, resp.; integral (12) now has the form

$$\frac{1}{4\pi} \int_0^{|\mathbf{r}_C - \mathbf{r}_{C'}'|} \int_0^D p_2(D, D') e^{-jkD'} dD' dD, \tag{15}$$

where $p_2(D, D') = \left(a + bD + D^2 + (c - D)D'\right)$ is a quadratic polynomial in D and D' with

$$\begin{aligned} a &= \left(\mathbf{r}_{C'}' - \mathbf{r}_i^e\right) \cdot \left(\mathbf{r}_{C'}' - \mathbf{r}_j^f\right), \\ b &= \hat{\mathbf{D}} \cdot (\mathbf{r}_{C'}' - \mathbf{r}_j^f + \mathbf{r}_{C'}' - \mathbf{r}_i^e), \\ c &= \hat{\mathbf{D}}' \cdot (\mathbf{r}_{C'}' - \mathbf{r}_i^e). \end{aligned} \tag{16}$$

The integral (12) or (15) is straightforwardly evaluated as

$$\frac{1}{4\pi} \left[\left(\left(\frac{a - c/(-jk)}{(-jk)^2} \right) + \left(\frac{b + c + 1/(-jk)}{(-jk)^2} \right) \left(D - \frac{1}{(-jk)} \right) \right) e^{-jkD} + \frac{(c/(-jk) - a)D - (b + 1/(-jk))D^2/2 - D^3/3}{(-jk)} \right]_{D=0}^{|\mathbf{r}_C - \mathbf{r}_{C'}'|}. \tag{17}$$

For the associated scalar potential radial integrals, the basis and testing functions are constants. Replacing a by that constant and dropping all terms not containing a in (15) and (17) yields the scalar potential radial integrals. For both scalar and vector potentials, the corresponding static potential result can either be evaluated directly or by evaluating (17) in the limit as $k \to 0$.

B. Numerical evaluation

We observe that the inner, radial integrals of (10) and (11) are over a triangular domain as shown in Fig. 4 (not to be confused with triangles S and S') and, since the singularity has been canceled, may be efficiently implemented as a surface integral over the domain using standard Gauss-triangle integration [17][18]. An exceptionally complete table of symmetrical rules for such integrals is available in [18]. For a Gauss-triangle quadrature rule with weights w_k^{GT} and barycentric coordinates $\xi_1^{GT(k)}$, $\xi_2^{GT(k)}$, $\xi_3^{GT(k)} = 1 - \xi_1^{GT(k)} - \xi_2^{GT(k)}$, $k = 1, \ldots, K$, the radial integral evaluation takes the form

$$\left[\int_0^{|\mathbf{r}_C-\mathbf{r}'_{C'}|}\int_0^D F(\mathbf{r},\mathbf{r}')\,D'dD'\,dD\right] \approx |\mathbf{r}_C-\mathbf{r}'_{C'}|^2\sum_{k=1}^{K} w_k^{GT} F\left(\mathbf{r}^{(k)},\mathbf{r}'^{(k)}\right)D'^{(k)}, \tag{18}$$

where

$$\mathbf{r}^{(k)}=\mathbf{r}'_{C'}+D^{(k)}\hat{\mathbf{D}},\quad D^{(k)}=\left(1-\xi_1^{GT(k)}\right)|\mathbf{r}_C-\mathbf{r}'_{C'}|,$$
$$\mathbf{r}'^{(k)}=\mathbf{r}^{(k)}+D'^{(k)}\hat{\mathbf{D}}',\quad D'^{(k)}=\xi_2^{GT(k)}|\mathbf{r}_C-\mathbf{r}'_{C'}|, \tag{19}$$
$$\hat{\mathbf{D}}=-\hat{\mathbf{D}}'=\frac{\mathbf{r}_C-\mathbf{r}'_{C'}}{|\mathbf{r}_C-\mathbf{r}'_{C'}|}.$$

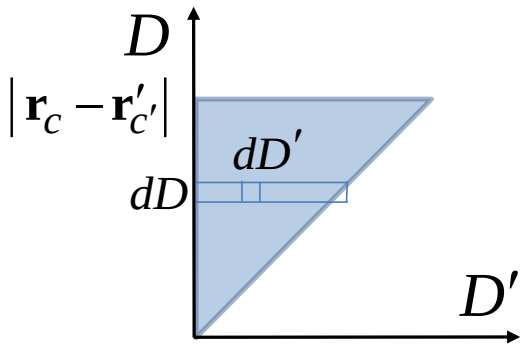

Figure 4. Triangular domain of integration for radial integrals.

In principle, the radial integral domains can be limited, as in (9), to regions interior to the source and observation triangles, thus saving points at which the kernel and bases need to be evaluated and eliminating cancellation errors from sample point contributions outside the original triangles that worsen as their separations increase. The approach may also be necessary for Green's functions with discontinuities outside the source testing domains, such as layered media Green's functions. However, more elaborate bookkeeping is needed to determine which and where triangle boundaries are crossed by the radial paths; such aspects will not be explored here.

C. Optimized numerical evaluation

For many problems, the radial integrals (12) take the form

$$\int_0^{|\mathbf{r}_C-\mathbf{r}'_{C'}|}\int_0^D \mathbf{\Lambda}_i^e(\mathbf{r})\cdot\mathbf{\Lambda}_j^f(\mathbf{r}')\,e^{-jkD'}\,dD'\,dD, \tag{20}$$

or have integrands bounded by integrands of this form, where basis and testing functions $\mathbf{\Lambda}_j^f(\mathbf{r}')$ and $\mathbf{\Lambda}_i^e(\mathbf{r})$, respectively, are assumed to be (vector) polynomials of order p in D' and D. Zhang et al. [18] provide a rather complete set of high-accuracy Gauss-type quadrature rules to exactly integrate 2-D polynomials of order ≤ 29 on the unit triangle. Hence, with an accuracy-based estimate of the polynomial order of the exponential phase factor $e^{-jkD'}$ over the domain, we can choose a quadrature rule that integrates the radial integrals to a *specified* number of decimal digits.

The exponential factor in (20) can be rewritten as

$$e^{-jkD'}=e^{-jk|\mathbf{r}_C-\mathbf{r}'_{C'}|/2}e^{-jk\left(D'-|\mathbf{r}_C-\mathbf{r}'_{C'}|/2\right)} =e^{-jk|\mathbf{r}_C-\mathbf{r}'_{C'}|/2}e^{-j\chi}=e^{-j\chi_{\max}}e^{-j\chi_{\max}x}, \tag{21}$$

where $\chi_{\max}=k|\mathbf{r}_C-\mathbf{r}'_{C'}|/2$, $\chi=x\chi_{\max}$, $-1\le x\le 1$, and we allow the medium wavenumber k to be complex. One might be tempted to use the truncated Taylor series error estimate to estimate the polynomial order of $e^{-j\chi_{\max}x}$ on the interval $-1\le x\le 1$, but we know that Taylor series errors usually increase rapidly away from the expansion point, with a maximum relative error at the endpoints. By contrast, an nth order Chebyshev polynomial spreads out the error, approximately minimizing the maximum error over the expansion interval, and indeed its error estimate is found to yield a much lower order estimate. The Chebyshev polynomial relative error estimate is [20]

$$\varepsilon_n=\left|\frac{e^{-j\chi_{\max}}\left(e^{-j\chi_{\max}x}-p_n(x)\right)}{e^{-j\chi_{\max}}e^{-j\chi_{\max}x}}\right| =\frac{\left|e^{j\chi_{\max}x}\right|}{2^n(n+1)!}\max_{x\in(-1,1)}\left|\frac{d^{n+1}e^{-j\chi_{\max}x}}{dx^{n+1}}\right|\le\frac{\left|\chi_{\max}\right|^{n+1}e^{2|\mathrm{Im}(\chi_{\max})|}}{2^n(n+1)!}. \tag{22}$$

where Im(z) denotes the imaginary part of z. Thus, the exponential factor (21) can be represented as a polynomial $p_n(x)$ of degree n to d significant decimal digits, if n is chosen such that

$$\varepsilon_n=\frac{2e^{|\mathrm{Im}(k)||\mathbf{r}_C-\mathbf{r}'_{C'}|}}{(n+1)!}\left(\frac{|k||\mathbf{r}_C-\mathbf{r}'_{C'}|}{4}\right)^{n+1}\le 10^{-d}. \tag{23}$$

The degree n satisfying (23) may be found iteratively using $\varepsilon_n=\frac{|\chi_{\max}/2|}{(n+1)}\varepsilon_{n-1}$ with $\varepsilon_0=2K|\chi_{\max}/2|e^{2|\mathrm{Im}(\chi_{\max})|}$, where $0<K<1$ is a parameter found to be about $K=0.75$ in numerical experiments. Finally, if basis and testing functions are both polynomials of order m, the integrands of the double radial integrals (15) or (20) can be replaced by $p_{2m}(D,D')e^{-jkD'}$, where $p_{2m}(D,D')$ is a polynomial of degree $2m$. In principle, one can then use either the method of the previous section to generate a closed form result analogous to (17), or if $e^{-jkD'}$ can be modeled as a polynomial of degree n with an error of less than 10^{-d}, the numerical approach of this section can be used to evaluate the radial integrals assuming an integrand of approximate degree $2m+n$. Thus increasing *either* the basis/testing order or the frequency simply raises the effective polynomial order of the integrand of the double radial integrals.

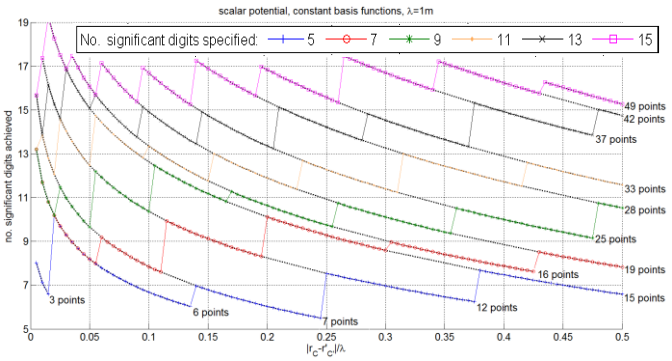

Figure 5. Number of correct significant digits vs. observation and source point separation normalized to wavelength, λ for scalar potential with constant basis functions, *k* real. Each curve corresponds to the number of (expected) significant digits specified in the quadrature rule. Curves connected by dashed lines all use the same number of sample points, with labels indicating the number used.

Figure 5 shows the actual number of correct significant digits obtained for the radial integrals (20) with respect to observation and source point separation in wavelengths, applying the proposed optimized radial integration quadrature rule. The case considered involves a scalar potential kernel with constant basis and testing functions, and real *k*. Each curve of Figure 5 corresponds to a specified number of significant digits, *d*, as input to the proposed procedure. Observe that, for each specified *d*, the achieved number of correct significant digits actually achieved is always at least as high as that specified, with the curve dipping to almost that value (with K adjusted to 0.75) just before the next higher order quadrature rule is invoked, suggesting the rule selection procedure is essentially optimal. Figure 5 also shows the solid lines connected by dotted lines and labeled to indicate the total number of sample points used for a fixed order quadrature rule. The curves suggest, for example, that six significant digits are always reached by a 7 point quadrature rule for observation and source points separated by no more than a quarter of a wavelength, a simple result that may be of practical use in a production code since it eliminates the need for solving (23). For vector potentials using linear (vector) bases, the order of the approximating integrand polynomial order should be increased by 2.

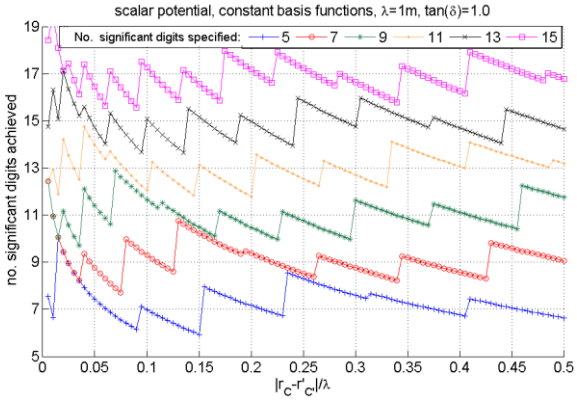

Figure 6. Number of correct significant digits vs. observation and source point separation normalized to wavelength, λ, for scalar potential with constant basis functions, *k* complex $\left(\mathrm{Im}(k) = -\mathrm{Re}(k)\right)$. Each curve corresponds to the number of (expected) significant digits specified in the quadrature rule.

Figure 6 reports results similar to those of Figure 5 but for a complex wavenumber k where $\mathrm{Im}(k) = -\mathrm{Re}(k)$, as is asymptotically the case for highly conducting materials. The behavior of the proposed optimized radial integration quadrature rule is similar to that for real *k*, but as might be expected, a few more sample points are required to reach the desired accuracy due to the exponential decay of the kernel. In this case, a detailed examination of the data shows that a 12 point rule will provide six significant digits of accuracy for observation and source points separated by no more than a quarter of a wavelength.

IV. CONTOUR INTEGRAL TRANSFORMATIONS

In order to improve numerical efficiency in evaluating the contour integrals in (11), we make transformations on the line integrals such that the two outer integrals become

$$\int_{\rho_L}^{\rho_U}\int_{\rho'_L}^{\rho'_U}[\,\cdot\,]\,d\rho'\,d\rho = \int_{u(\rho_L)}^{u(\rho_U)}\left[\int_{u'(\rho,\rho'_L)}^{u'(\rho,\rho'_U)}[\,\cdot\,]\frac{du'}{\partial u'/\partial\rho'}\right]\frac{du}{du/d\rho}, \qquad (24)$$

where $\partial u'/\partial\rho'$ is chosen to largely cancel variations in the inner bracketed integrand resulting from the two radial integrations, and $du/d\rho$ plays the same role for the resulting outer bracketed integral in (24). A sufficiently accurate estimate of the required smoothing for kernels with singularities of order $\mathcal{O}\left(1/|\mathbf{r}-\mathbf{r}'|\right)$ can be obtained by using the *static* integrand with constant basis and testing functions as a model integrand, i.e., we temporarily assume

$$F(\mathbf{r},\mathbf{r}') \approx \frac{1}{4\pi|\mathbf{r}-\mathbf{r}'|}. \qquad (25)$$

To put the necessary integrations in standard form for all triangle edge pairs, we assume a rotation of the triangle plane until the relevant source edge is horizontal and directed to the right as shown in Figure 7. We further assume that the extended edges of the edge pair intersect at an angle α as shown; the arc length variables ρ and ρ' parameterize the edges in (24), and are measured from the intersection point of the (extended) line segments. For parallel line segments, the intersection point and the parameters ρ and ρ' become infinite, $\alpha = 0$ or $\pm\pi$, and the case must be treated as a limit. Calculation of the intersection point and other relevant geometry considerations are discussed in Appendix A. Parallel line segments are treated in both Appendices A and B.

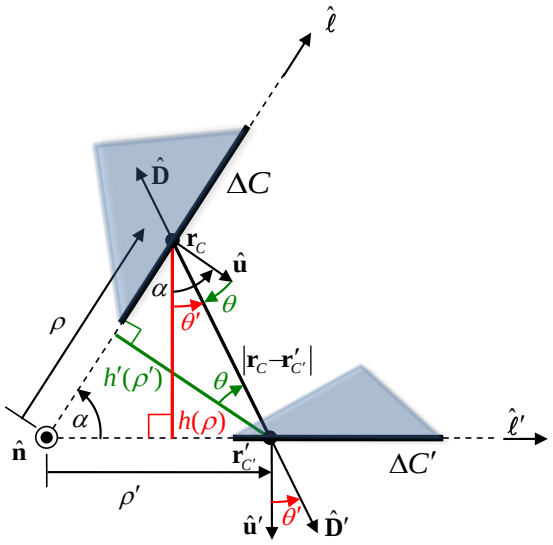

Figure 7. Geometry for integrating over a line segment pair.

With (25), the radial integrals can be easily performed, resulting in

$$\frac{(\hat{\mathbf{u}}\cdot\hat{\mathbf{D}})(\hat{\mathbf{u}}'\cdot\hat{\mathbf{D}}')}{8\pi}|\mathbf{r}_C-\mathbf{r}'_{C'}| \tag{26}$$

for the term in the (inner) square brackets in (24). Noting from Figure 7 that

$$\theta=\alpha-\theta', \tag{27}$$

and that

$$\begin{aligned}\hat{\mathbf{u}}'\cdot\hat{\mathbf{D}}'&=\cos\theta'=\frac{h(\rho)}{R(\rho,\rho')}=\frac{\rho\sin\alpha}{R(\rho,\rho')}=-\frac{\hat{\mathbf{u}}'\cdot(\mathbf{r}_C-\mathbf{r}'_{C'})}{|\mathbf{r}_C-\mathbf{r}'_{C'}|},\\ \hat{\mathbf{u}}\cdot\hat{\mathbf{D}}&=-\cos\theta=-\frac{h'(\rho')}{R(\rho,\rho')}=-\frac{\rho'\sin\alpha}{R(\rho,\rho')}=\frac{\hat{\mathbf{u}}\cdot(\mathbf{r}_C-\mathbf{r}'_{C'})}{|\mathbf{r}_C-\mathbf{r}'_{C'}|},\end{aligned} \tag{28}$$

where

$$|\mathbf{r}_C-\mathbf{r}'_{C'}|=R(\rho,\rho')=\sqrt{\rho^2+\rho'^2-2\rho\rho'\cos\alpha}\,, \tag{29}$$

(26) can be written as

$$\frac{(\hat{\mathbf{u}}\cdot\hat{\mathbf{D}})(\hat{\mathbf{u}}'\cdot\hat{\mathbf{D}}')}{8\pi}|\mathbf{r}_C-\mathbf{r}'_{C'}|=-\frac{\rho\rho'\sin^2\alpha}{8\pi\sqrt{\rho^2+\rho'^2-2\rho\rho'\cos\alpha}}\,. \tag{30}$$

With the choice

$$\frac{\partial u'}{\partial\rho'}=\frac{\rho'\sin\alpha}{\sqrt{\rho^2+\rho'^2-2\rho\rho'\cos\alpha}}=\frac{h'(\rho')}{R(\rho,\rho')}=\cos\theta, \tag{31}$$

the variation of the inner line integral for the static kernel is exactly canceled; integration of (31) yields

$$u'(\rho,\rho')=\sin\alpha R(\rho,\rho')+h(\rho)\cos\alpha\sinh^{-1}\left(\frac{\rho'-\rho\cos\alpha}{|h(\rho)|}\right). \tag{32}$$

Combining (30) and (31) with (25), (11), and (24) yields

$$\begin{aligned}&\int_{\rho_L}^{\rho_U}\int_{\rho'_L}^{\rho'_U}\left[\frac{(\hat{\mathbf{u}}\cdot\hat{\mathbf{D}})(\hat{\mathbf{u}}'\cdot\hat{\mathbf{D}}')}{|\mathbf{r}_C-\mathbf{r}'_{C'}|}\int_0^{|\mathbf{r}_C-\mathbf{r}'_{C'}|}\int_0^D F(\mathbf{r},\mathbf{r}')\,D'dD'\,dD\right]d\rho'd\rho\\ &=\frac{-1}{8\pi}\int_{\rho_L}^{\rho_U}\int_{\rho'_L}^{\rho'_U}\frac{\rho\rho'\sin^2\alpha}{R(\rho,\rho')}d\rho'd\rho\\ &=\frac{-1}{8\pi}\int_{\rho_L}^{\rho_U}\left[h(\rho)\int_{u(\rho,\rho'_L)}^{u(\rho,\rho'_U)}du'\right]d\rho\\ &=\frac{-1}{8\pi}\int_{\rho_L}^{\rho_U}h(\rho)\left[u'(\rho,\rho'_U)-u'(\rho,\rho'_L)\right]d\rho\,.\end{aligned} \tag{33}$$

The integrand of (33) suggests choosing

$$u(\rho)=\tilde{u}(\rho,\rho')\Big|_{\rho'=\rho'_L}^{\rho'_U}\,, \tag{34}$$

where

$$\begin{aligned}\frac{\partial\tilde{u}(\rho,\rho')}{\partial\rho}&=h(\rho)u'(\rho,\rho')\\ &=h(\rho)\left[\sin\alpha\,R(\rho,\rho')+h(\rho)\cos\alpha\sinh^{-1}\left(\frac{\rho'-\rho\cos\alpha}{|h(\rho)|}\right)\right]\end{aligned} \tag{35}$$

since

$$\frac{du}{d\rho}=\frac{\partial\tilde{u}(\rho,\rho')}{\partial\rho}\Big|_{\rho'=\rho'_L}^{\rho'_U}=h(\rho)\left[u'(\rho,\rho'_U)-u'(\rho,\rho'_L)\right] \tag{36}$$

then reproduces the integrand of (33), yielding

$$\begin{aligned}&\int_{\rho_L}^{\rho_U}\int_{\rho'_L}^{\rho'_U}\left[\frac{(\hat{\mathbf{u}}\cdot\hat{\mathbf{D}})(\hat{\mathbf{u}}'\cdot\hat{\mathbf{D}}')}{|\mathbf{r}_C-\mathbf{r}'_{C'}|}\int_0^{|\mathbf{r}_C-\mathbf{r}'_{C'}|}\int_0^D F(\mathbf{r},\mathbf{r}')\,D'dD'\,dD\right]d\rho'd\rho\\ &=-\frac{1}{8\pi}\left[\tilde{u}(\rho_U,\rho'_U)-\tilde{u}(\rho_U,\rho'_L)-\tilde{u}(\rho_L,\rho'_U)+\tilde{u}(\rho_L,\rho'_L)\right]\end{aligned} \tag{37}$$

for $F(\mathbf{r},\mathbf{r}')$ the static kernel (25). Thus, if (36) can be integrated, Eq. (37) furnishes for the static kernel (25) a closed form result for the reaction between each line integral pair, and, by superposition, for the entire double surface integral. Details for integrating (36) are found in Appendix B; the result is

$$\begin{aligned}\tilde{u}(\rho,\rho')&=\sin^2\alpha\left[\rho^2+\rho'^2\right]\frac{R(\rho,\rho')}{3}\\ &+\frac{h'(\rho')^3}{3\tan\alpha}\sinh^{-1}\left(\frac{\rho-\rho'\cos\alpha}{|h'(\rho')|}\right)\\ &+\frac{h(\rho)^3}{3\tan\alpha}\sinh^{-1}\left(\frac{\rho'-\rho\cos\alpha}{|h(\rho)|}\right).\end{aligned} \tag{38}$$

Though $\tilde{u}(\rho,\rho')$ is bounded, for α near zero or $\pm\pi$, the last two terms of (38) become very large, nearly equal, and of opposite sign, leading to large cancellation errors. Also, for parallel line segments, $\alpha\to 0,\pm\pi$, (38) must be evaluated as a limit. Both situations are handled by replacing the last two terms of (38) by Taylor series expansions about $\alpha=0$ and

$\alpha = \pm\pi$, which simultaneously incorporates the limits and eliminates cancellation error in the vicinity of these values. The relevant series approximations are derived in Appendix B.

We note that the integrand (24) is generally a function of ρ' and ρ whereas the numerical integration is in the u' and u domains. Hence inverse functions or mappings of the transcendental functions u' and u back to ρ' and ρ are needed. Since u' and u depend on edge pair geometry, the inverse mappings differ, in general, for each point pair associated with a given edge pair. Fortunately, continuous mappings are not required, however, since the quadrature rules only require discrete values of u' and u. E.g., for the kth sample point $u' = u'_k$, the corresponding value $\rho' = \rho'_k$ may be efficiently found via a simple Newton scheme that determines the root ρ'_k of the equation $u'(\rho, \rho'_k) - u'_k = 0$, as in [11]. The derivative of the inverse transform is $d\rho'/du' = 1/\left(\partial u'(\rho,\rho')/\partial\rho'\right)$ and for u' between the two values $u'(\rho,\rho'_U), u'(\rho,\rho'_L)$, the inverse exists as long the derivative $\partial u'/\partial\rho'$ is non-vanishing on the interval, which, from (31), is clearly the case as long as $\rho' \neq 0$. Unfortunately, in the MoM, this exceptional case occurs rather frequently for realistic triangles, e.g. for *all* edge pairs of a self-term. More generally, it occurs whenever extended source and test line segments intersect at an endpoint or interior point of the source segment. A simple means for detecting this situation is given in Appendix A. If $\rho' = 0$ is an endpoint of the source segment, special treatment of the line segment integral is required, as outlined below; if $\rho' = 0$ is an interior point, the integration domain should be split into two subdomains about the point $\rho' = 0$ and the following treatment applied on each line sub-segment.

To analyze the behavior of u' near $\rho' = 0$, we note transformation (32) can be expanded in a Maclaurin series, obtaining

$$u'(\rho,\rho') = u'_0 + \frac{\rho'^2}{2|\rho|}\sin\alpha + \mathcal{O}(\rho'^3), \tag{39}$$

where $u'_0 \equiv u'(\rho,0)$. The inverse function corresponding to (39) thus has a square root type branch point at $u' = u'_0$,

$$\rho' \approx \pm\sqrt{\frac{2|\rho|}{|\sin\alpha|}}\sqrt{\mathrm{sgn}(\sin\alpha)(u'-u'_0)}. \tag{40}$$

Note that in (40), $\sin\alpha$ and $(u'-u'_0)$ must have the same sign near $\rho' = 0$. The branch point may thus be removed by introducing the secondary transformation

$$v'^2 = \mathrm{sgn}(\sin\alpha)(u'-u'_0), \tag{41}$$

not only eliminating the branch point in the source contour integrand, but also, since $2v'dv' = \mathrm{sgn}(\sin\alpha)du'$, introducing a zero in the new integration variable v' where the denominator factor $\partial u'/\partial\rho'$ in (24) vanishes. Similarly, examination of the behavior of the transformation (34) near $\rho = 0$ yields the Maclaurin series

$$\begin{aligned} u(\rho) &= \tilde{u}(\rho,\rho'_U) - \tilde{u}(\rho,\rho'_L) \\ &= u_0 + \tfrac{1}{2}\rho^2\sin^2\alpha\left(|\rho'_U| - |\rho'_L|\right) + \mathcal{O}(\rho'^3) \end{aligned} \tag{42}$$

where $u_0 = \tilde{u}(0,\rho')\big|_{\rho'=\rho'_L}^{\rho'_U}$. Hence the secondary transform

$$v^2 = \mathrm{sgn}\left(|\rho'_U| - |\rho'_L|\right)(u - u_0), \tag{43}$$

eliminates a similar square root type branch point in the test contour integrand, and introduces a zero in v where the denominator factor $du/d\rho$ of (24) vanishes. The overall scheme for using the transforms may now be summarized as follows:

- Select a source and test edge pair and check if they are (anti-)parallel. If so, then skip calculation of the pair's interaction, and proceed to the next pair.

- Examine the source and test edge pairs for endpoints that occur at the intersection of their extended line segments; if an intersection occurs *within* a line segment, the segment should be divided into two subsegments, and each treated as an independent edge. For segments or subsections with an end-point at the intersection, the associated u or u' transform should be followed by a v or v' transform, as appropriate.

- Select a quadrature rule and use it to discretize v (v') or u (u'), as appropriate, for each line segment. If v (v') parameterizes the line segment, then each sample point $v^{(k)}$ ($v'^{(k')}$) is mapped directly back to the corresponding point $u^{(k)}$ ($u'^{(k')}$). Otherwise, use the quadrature rule to directly select the sample points $u^{(k)}$ ($u'^{(k')}$).

- Map points $u^{(k)}$ ($u'^{(k')}$) back to discrete sample points $\ell^{(k)} = \rho^{(k)} - \rho_L$ ($\ell'^{(k')} = \rho'^{(k')} - \rho'_L$) in the local line segment arc length parameter (see Appendix A) using Newton's method to solve $u(\ell^{(k)}) - u^{(k)} = 0$ ($u'(\ell, \ell'^{(k')}) - u'^{(k')} = 0$). The integrands of the contour integrals are then evaluated at the test and source contour points $\ell^{(k)}$ and $\ell'^{(k')}$, respectively.

We also remark that as an alternative to the proposed secondary transforms (41) and (43), the quadrature scheme of Ma, Rockhlin and Wandzura for square root singularities [21][22] can be used directly for the ρ and ρ' integrations whenever $\rho = 0$ and/or $\rho' = 0$ are end or interior points of the integration domain. Note the transformations (32) and (38) make the integrand analytic only for pulse basis functions and static kernels. For higher order basis functions and dynamic kernels, the dominant singularities of the integrands are removed but the integrands are not analytic, thus creating the

need for quadratures that treat other singularities such as the Ma, Rockhlin and Wandzura quadratures and the double exponential quadrature schemes used to produce the numerical results of the next section.

Finally, we note that the choices (31) and (32) cancel the rapid variation of $\hat{\mathbf{u}}\cdot\hat{\mathbf{D}}$ in the integrand; this approach can also be extended to cancel just the dual factor $\hat{\mathbf{u}}'\cdot\hat{\mathbf{D}}'$, leading to a dual expression for u (i.e., with primed and unprimed quantities interchanged). In limited testing, this alternative transform pair has been found to work almost as well as the approach described, is simpler, and is symmetric with respect to its treatment of source and test contour integrals.

V. Numerical Results

In this section, we examine the numerical characteristics of the proposed approach. It is both convenient and instructive to separately examine convergence of the edge pair contour and radial integrals representing contributions to the reactions between triangular element pairs. Hence, to study convergence of the contour integrals, we use the exact result (17) for the radial integrals to eliminate that source of error; on the other hand, when studying the radial integral convergence, we use a very accurate, double exponential (DE) quadrature rule [9] to assure that the contour integrals are well-converged. To obtain reference values for determining the reaction integral error, we use the exact radial integral together with a high order DE rule for the contour integrals. In obtaining reference values, calculations are performed in quad precision using comparable precision quadrature data and root-finding tolerances; all reference values used have been found accurate to at least 25 significant digits. All other computations are performed in double precision.

For vector potential reaction integrals, all nine linear edge basis and test function reaction combinations are computed for a triangle pair, and the worst case result (least number of significant digits) is reported. For scalar or static potential quantities, we assume constant bases and report a single result.

For each type of reaction integral considered, the error metric reported is the number of significant digits (SD) of the computed reaction integral,

$$\mathrm{SD} = -\log_{10}\left(\left|(I_{\mathrm{ref}} - I_n)/I_{\mathrm{ref}}\right| + \delta\right), \qquad (44)$$

where I_n is the integral computed using n sample points, and the reference value is I_{ref}. Since the working precision of our computations is double precision, the term $\delta = 1.0\mathrm{E}{-16}$ is added in the argument of the logarithm to ensure that precision beyond 16 significant digits is neither claimed nor reported. Fig. 8 shows the accuracy of vector potential self-reaction integrals for coincident source and test triangles that are right isosceles triangles with perpendicular sides each of length 0.1λ. (For this and other cases where the scalar potential is unreported and where triangle pairs have maximum edge lengths of 0.1λ, the scalar potential was always found to converge to 2–3 more significant digits than the vector potential for a given number of sample points. Figures 9, 11, 13, and 15 illustrate this point.) The exact result (17) is used for the radial integrals in Fig. 8, and two quadrature schemes, Gauss-Legendre (GL) and double exponential (DE), are compared. The number of sample points per edge contour integral is the same for both test and source edges, and the number of significant digits obtained is plotted vs. this quantity. As is typical when using these two quadrature rules, GL appears more effective at achieving low-to-moderate accuracies, whereas the DE scheme is effective when very high accuracies are desired. The quadrature schemes' behavior is also compared with and without the integrand-smoothing contour transforms. For self terms, since every edge pair intersects the endpoint of another edge, when using transforms for the contour integrals, not only the u and u' transforms, but also the v and v' transforms must be invoked for each edge pair. The effectiveness of the contour integral transforms is clear: in the GL scheme, for a specified accuracy, about half as many sample points are needed per edge (or about one quarter the total number of points per edge pair). Higher accuracies can be achieved using the DE scheme, where the effectiveness of the contour integral transforms is even more pronounced. It is noteworthy that for self terms, there are only 6 non-vanishing edge pair combinations, but only 3 of them are independent. Therefore the total number of sample points used in Fig. 8 may be closely estimated as $3N_{\mathrm{E}}^2 N_{\mathrm{R}}$ where N_{E} represents the horizontal axis of the figure, i.e. the number of sample points for both source and test edges for the 3 interacting pairs of the 9 edge pairs (6 pairs are collinear and hence do not interact); N_{R} is the number of sample points used for radial integration. Hence combining a relatively low order GL quadrature rule with exact radial integration (i.e., $N_{\mathrm{R}} = 1$) can lead to a very efficient and accurate self term evaluation suitable for many applications.

For numerical radial integration, an optimum N_{R} corresponding to a given number of significant digits in Fig. 6 can be closely estimated using Fig. 5 with $|\mathbf{r}_C - \mathbf{r}'_{C'}|/\lambda = \sqrt{2}/10$, corresponding to the longest triangle side.

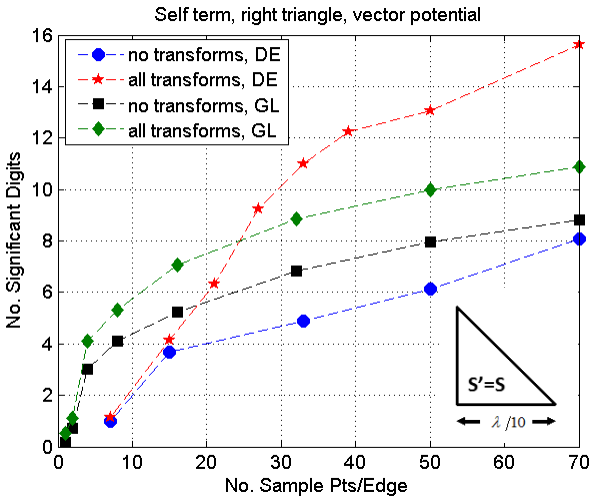

Figure 8. Number of correct significant digits vs.number of sample points per edge; vector potential, self term case for right isosceles triangle. Gauss-Legendre (GL) and double exponential (DE) quadrature rules with and without variable transforms are compared; the radial integration is exact.

In Fig. 9, for the same situation considered in Fig. 8, a very high order DE quadrature rule is used to ensure the

convergence of the contour integrals, and Gauss-triangle rules [18] are applied to the radial integral. The number of radial quadrature points, N_R, shown is the total for the triangular integration domain of Fig. 4. The scalar potential integral apparently converges to about 2 more significant digits than the vector potential integral. Recall that for the radial integral, it is also possible to specify the number of significant digits desired and use (23) to select the appropriate Gauss-triangle quadrature rule [18]. We also note in Fig. 9 that only one radial sample point per edge pair is required to integrate the static scalar potential to machine precision; this is also true for each of the *contour* integrals when the *u* and *u'* transforms are used since they are chosen to exactly integrate the static kernel.

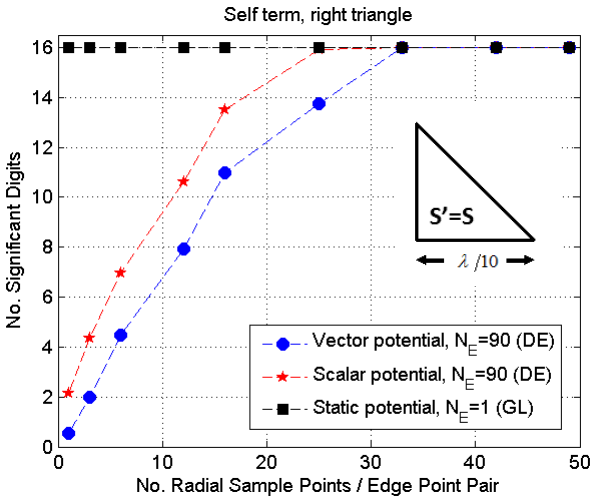

Figure 9. Number of correct significant digits vs. number of radial sample points for each edge point-pair integral; self term case for right isosceles triangle; vector, scalar and static potential; N_E = number of sample points per edge (contour integrals).

In Figs. 10–13 the same analysis is performed for edge-adjacent and vertex-adjacent cases using the same coplanar source and test triangles as for the self term case, but positioned as shown in the corresponding inserts. The total number of sample points used in Figs. 10–13 may be closely estimated as $8N_E^2N_R$ since in both cases one pair of the 9 edge pairs is collinear. It is evident that the accuracy behavior of the contour and radial integrals is very similar to the results obtained for the self term case. However, comparing Figs. 9, 11, and 13 for the radial integrals, we see that as the triangles are moved apart, convergence is slightly slower due to the relatively longer electrical distances between source and test triangle edge pairs. Also note that, due to the presence of the linearly-varying basis and test functions in the vector potential, the vector potential loses about two significant digits of accuracy compared to the scalar potential, where constant bases are used.

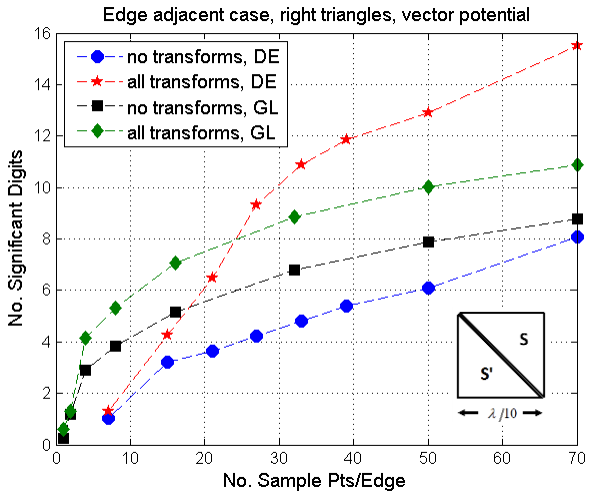

Figure 10. Number of correct significant digits vs. number of sample points per edge; vector potential edge adjacent case with right isosceles triangles. Gauss-Legendre (GL) and double exponential (DE) quadrature rules with and without variable transforms are compared; the radial integration is exact.

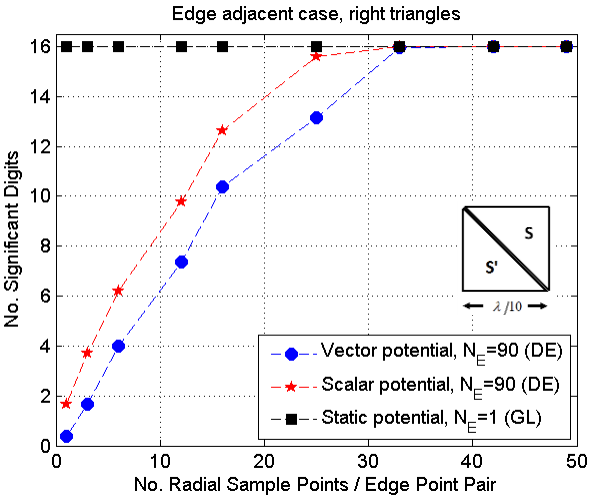

Figure 11. Number of correct significant digits vs. number of radial sample points for each edge point-pair integral; edge adjacent case with right isosceles triangles; vector, scalar and static potential; N_E = number of sample points per edge (contour integrals).

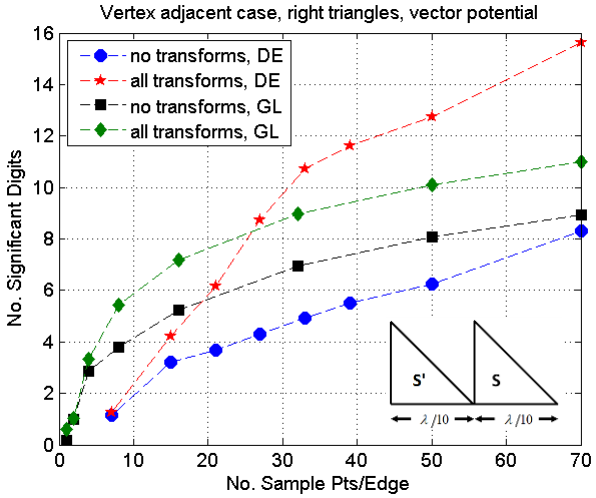

Figure 12. Number of correct significant digits versus number of sample points per edge; vector potential vertex adjacent case with right isosceles triangles. Gauss-Legendre (GL) and Double Exponential (DE) quadrature

rules with and without variable transforms are compared; the radial integration is exact.

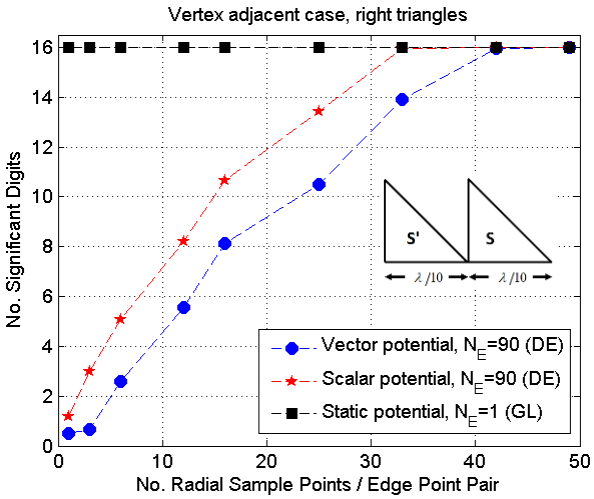

Figure 13. Number of correct significant digits vs. number of radial sample points for each edge point-pair integral; vertex adjacent case with right isosceles triangles; vector, scalar and static potential; N_E = number of sample points per edge (contour integrals).

In Figs. 14 and 15 the same analysis is performed for the non-touching test and source triangle pair shown in the inserts. The total number of sample points for non-touching triangles with *no* collinear edges is generally $9N_E^2N_R$; in this case, however, there are $8N_E^2N_R$ sample points since there is one collinear edge pair. The accuracy results for the contour integrals (Fig. 14) are quite different from the previous cases since, with well-separated edge pairs, the integrand is sufficiently smooth that the Gauss-Legendre quadrature rule is effective even without transforming the contour integrals or using the DE scheme.

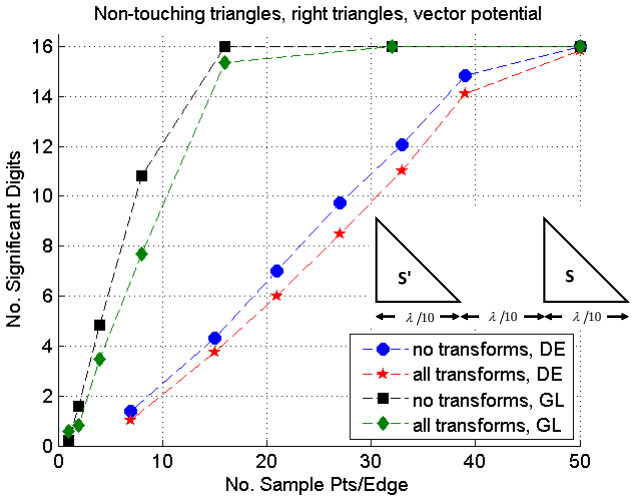

Figure 14. Number of correct significant digits vs. number of sample points per edge; case of non-touching right isosceles triangles. Gauss-Legendre (GL) and Double Exponential (DE) quadrature rules with and without variable transforms are compared; the radial integration is exact.

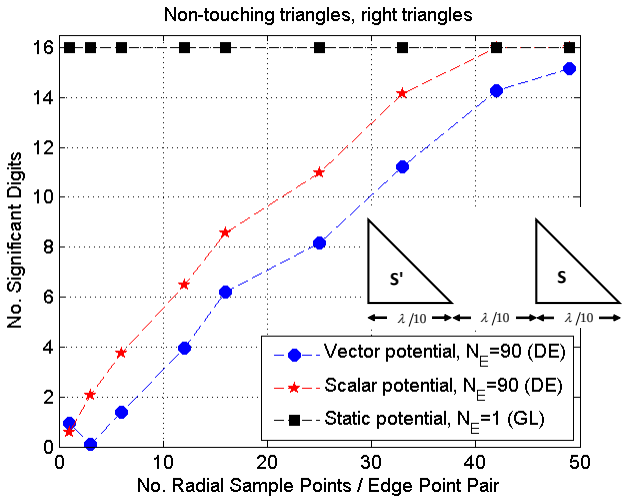

Figure 15. Number of correct significant digits vs. number of radial sample points for each edge point pair integral; non-touching right isosceles triangles; vector, scalar and static potential; N_E = number of sample points per edge (contour integrals).

An advantage of (10) for performing 4-D integrals on triangle pairs is its relative insensitivity to triangle shapes, which is even further improved by transforming the edge integrals using (32), (34) and (38). The error contour plots in Fig. 16 show (using a common color bar key) the number of correct significant digits in the scalar potential self term for different shaped triangles. The endpoints 1 and 2 of a triangle's longest edge are placed at points 0.0 and 1.0 along the x-axis, respectively (since it is symmetric, only the left half of each plot is shown); the third vertex can then only appear within or on the boundary of the region bounded by two circular arcs centered at vertices 1 and 2 and with radii equal to the maximum edge length [13] (i.e., any point *outside* the region has at least one edge longer than the maximum). The frequency is chosen such that the electrical length of the longest edge is $\lambda/10$; the plot region thus embraces triangles of *any* shape whose maximum edge length is $\lambda/10$. The color at each point (x,y) is keyed to the number of correct significant digits for a triangle with its third vertex at the point. The number of sampling points per edge is 8 and the total number of radial sample points is fixed at 7 (sufficiently accurate for all radial paths), and GL quadrature is used. The contour plot of Fig. 16(a) shows the accuracy obtained applying all the proposed transforms; Fig. 16(b) shows the same without transforms. As the figure clearly shows, the transforms counteract the effects of rapid variations of the dot product terms in (10) that occur for nearly parallel edges, making accuracy relatively insensitive to triangle shape.

For homogeneous medium kernels, we have found that using the transforms can result in a CPU time penalty factor of about 6 for well-shaped triangles and for the same number of edge sample points. Indeed, the extra computational burden of the transform evaluation and root finding almost negates the gain resulting from the decreased number of sampling points needed to achieve a given accuracy. However, for very poorly-shaped triangles, it is very difficult to achieve desired accuracies *without* the transforms, so that the required CPU time for a given accuracy is much reduced using the transforms. Hence, for the homogeneous medium kernel, one

can say that a principal benefit of the transforms is to ensure relative insensitivity to triangle shape. And for problems involving certain Green's functions, such as those for periodic and/or layered media where kernel evaluation costs are typically hundreds of times greater than for homogeneous media kernels, one should expect that the extra overhead of computing transforms and their inverses is practically negligible compared to the time saved by needing fewer kernel evaluations.

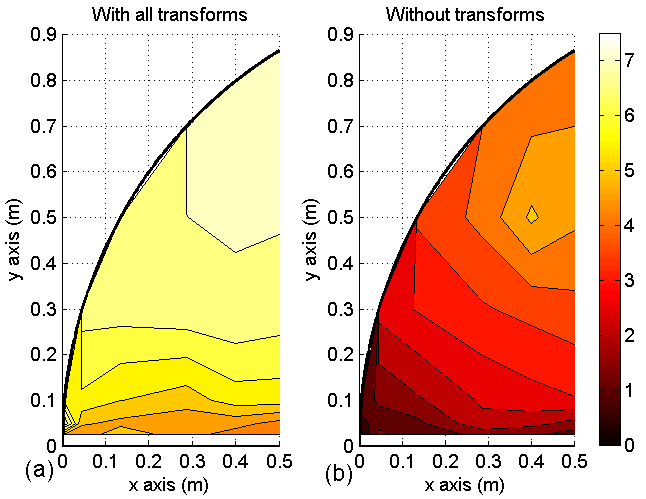

Figure. 16. Significant digits for scalar potential, self term, vs. triangle shape for a triangle whose longest edge is length = λ/10, and with vertices 1 and 2 at $(x,y) = (0,0)$ and $(x,y) = (1,0)$, respectively. The color at any point (x,y) locating vertex 3 is keyed to the colorbar showing the number of correct significant digits for that triangle shape with (a) all transforms applied and (b) no transforms applied. Number of sample points per edge $N_E = 8$ (GL quadrature rule); number of radial sample points per edge pair $N_R = 7$ (Gauss-triangle rule).

In Fig. 17, for the vector potential of a self element case, the proposed scheme (blue line with circle markers) is compared with the Radial-Angular (RA) singularity cancellation scheme [13] for source integration combined with test integration using Gauss-Legendre (GL, red line with star or square markers) and Ma-Rokhlin-Wandzura [21,22] quadrature schemes (MRW-log, green line with up- or down-pointing triangle markers). The latter is appropriate for integrands that can be approximated as a polynomial plus the product of a polynomial and a logarithm function. As discussed in [14], the MRW-log scheme is appropriate for this case when high accuracy in the testing integral is desired.

The RA scheme is currently regarded as among the most efficient source integral schemes [12]. Usually for the associated test integrations, a simple Gauss-Triangle or GL product rule is used in the RA. But as discussed in [14], for very high accuracy test integrations near source element edges, a MRW-log quadrature scheme should be used since potentials have a $\rho \ln \rho$ variation very near the edges, with ρ representing distance from an edge. This singular behavior is tightly confined to a small region near the edges, however, as evidenced by the fact that ordinary GL initially outperforms the MRW-log scheme up to about four significant digits (RA opt, star or down-pointing triangle markers). However, this trend reverses as test sample points are pushed closer to the edges of the source triangle. The testing integration is evaluated using standard GL product rules varying the number of sample points from 7 to 61 (star or square markers) or using MRW-log product rules, varying the number of sample points from 8 to 50 for each of the three sub-triangles into which the test triangle is subdivided [14]. That the underlying RA scheme is largely limited by the test integral accuracy is seen by increasing the source quadrature (RA opt+1, rectangular or up-pointing triangle markers); the results are merely shifted horizontally to the right with essentially no increase in accuracy.

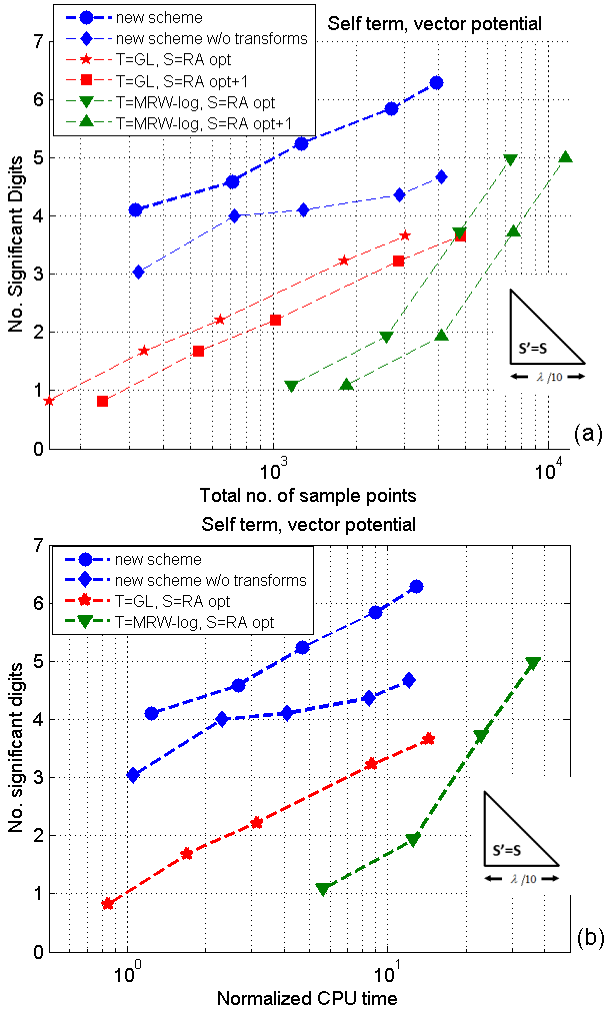

Figure 17. Number of correct significant digits (a) vs. total no. of sample points and (b) vs. normalized CPU time. Vector potential, self element for a right isosceles triangle whose perpendicular sides are of length λ /10 comparing present scheme to Radial-Angular (RA) singularity cancellation scheme [13] for the source triangle (S) using Gauss-Legendre (GL) or Ma-Rokhlin-Wandzura (MRW-log) quadrature schemes for the test integral (T).

Figure 17(a) compares the number of significant digits vs. the total number of sample points required to evaluate vector potential for a right isosceles triangle. Comparison is with respect to schemes reported in [13]. Figure 17(b) presents the same data vs. normalized CPU time. Times reported are normalized with respect to the time required to perform 100 evaluations of the 9 vector potential integrals divided by the time required to perform the same evaluation simply applying a GL quadrature scheme with 16 sample points to the traditional surface/surface test and source integrals.

The most important observation in Fig. 17 is the superior efficiency of the proposed scheme in minimizing the number of sample points compared to the RA scheme, either with or without transforms. To generate the data for the proposed scheme, a form of "manual optimization" of the radial sampling has been used: For each case, the 4-D integral is first evaluated using the *exact* radial integral (17) and with a selected contour sample point scheme. The number of significant digits obtained is then rounded to the next higher integer, and this number is used in the scheme of Sect. III.C to select the appropriate radial sampling scheme that *numerically* evaluates the integral to the same accuracy. The resulting number of significant digits and total number of kernel sample points in this latter case are reported in Fig. 17.

For the cases considered, it is evident that the proposed scheme is more efficient with respect to number of sample points required for a specified accuracy than some commonly-used singularity cancellation schemes coupled with appropriate testing schemes. It is also more efficient than the scheme of [1], though we emphasize that the latter was not optimized in any way. Overall calculation time will also be reduced whenever the time saved in kernel evaluations heavily outweighs the method's slightly increased overhead for computing transforms and their inverse mappings at sample points.

VI. Conclusions

We present a novel general formula for 4-D reaction integrals involving coplanar elements based on a double application of the surface divergence theorem. The representation obtained has two inner radial integrals and two outer contour integrals over the source and test element boundaries. The method's efficiency, in terms of number of correct significant digits for a given kernel sampling rate and its insensitivity to triangle shape, is strongly improved by employing variable transforms for the contour integrals to further smooth the integrands and accelerate convergence of the integrals. Moreover, a closed form evaluation of the radial integrals is derived for a homogeneous medium kernel and standard linear triangle basis and testing functions; alternatively, for a completely numerical approach, a scheme is developed to optimize the choice of quadrature rule.

The next step in this research activity is to extend the approach to non-coplanar elements and to kernels having other singularities. It also appears the approach can be extended to curved elements.

Acknowledgments

The authors wish to acknowledge many fruitful discussions with Athanasios Polimeridis. They also wish to thank Javier Rivero for his assistance in performing the calculations.

References

[1] A. G. Polimeridis, F. Vipiana, J. R. Mosig, and D. R. Wilton, "DIRECTFN: Fully Numerical Alogorithms for High Precision Computation of Singular Integrals in Galerkin SIE Methods," *IEEE Trans., Ant. and Propagat.*, 61,6, 2013.pp. 3112–3122.

[2] A. G. Polimeridis and T. V. Yioultsis, "On the direct evaluation of weakly singular integrals in Galerkin mixed potential integral equation formulations," *IEEE Trans. Antennas Propagat.*, vol. 56, 9, pp. 3011–3019, Sep. 2008.

[3] A. G. Polimeridis and J. R. Mosig, "Complete semi-analytical treatment of weakly singular integrals on planar triangles via the direct evaluation method," *Int. J. Numer. Meth. Eng*., vol. 83, pp. 1625–1650, 2010.

[4] A. G. Polimeridis, J.M. Tamayo, J. M. Rius, and J. R. Mosig, "Fast and accurate computation of hyper-singular integrals in Galerkin surface integral equation formulations via the direct evaluation," *IEEE Trans. Antennas Propagat.*, vol. 59, no. 6, pp. 2329–2340, Jun. 2011.

[5] A. G. Polimeridis and J. R.Mosig, "On the direct evaluation of surface integral equation impedance matrix elements involving point singularities," *IEEE Antennas Wireless Propagat. Lett.*, vol. 10, pp. 599–602, 2011.

[6] D. R. Wilton, S. M. Rao, A. W. Glisson, D. H. Schaubert, O. M. Al-Bundak, and C. M. Butler, "Potential Integrals for Uniform and Linear Source Distributionss on Polygonal and Polyhedral Domains," *IEEE Trans. Antennas Propagat.*, vol. 32, 3, Mar. 1984, pp. 276–281.

[7] P. Arcioni, M. Bressan, and L. Perregrini, "On the Evaluation of the Double Surface Integrals Arising in the Application of the Boundary Integral Method to 3-D Problems," *IEEE Trans. Microwave Theory Tech*., vol. 45, 3, Mar. 1997, pp. 436–439.

[8] L. Knockaert, "On the analytic calculation of multiple integrals in electromagnetics," Proc. ICEAA, Torino (Italy), Sept. 2011.

[9] A. G. Polimeridis, I. D. Koufogiannis, M. Mattes, J. R. Mosig, "Considerations on Double Exponential-Based Cubatures for the Computation of Weakly Singular Galerkin Inner Products," *IEEE Trans. Antennas Propagat.*, vol. 60, 5, May 2012, pp. 2579–2582.

[10] D. R. Wilton, F. Vipiana, W. A. Johnson, "Fully numerical evaluation of singular integrals in Moment methods: A novel strategy for the coplanar element case," Proc. Radio Science Meeting (Joint with AP-S Symposium), Memphis (TN, USA), July 2014, p.190.

[11] F. Vipiana and D. R. Wilton, "Numerical Evaluation via Singularity Cancellation Schemes of Near-Singular Integrals Involving the Gradient of Helmholtz-Type Potentials," *IEEE Trans. Antennas Propagat.*, vol. 61, 3, Mar. 2013, pp. 1255–1265.

[12] M. Botha, "Accuracy of near-singularity cancellation quadrature schemes for the dynamic MoM kernel," *IEEE Antennas Wirel. Propagat. Lett.*, vol. 12, May 2013, pp. 714–717.

[13] M. A. Khayat, D. R. Wilton, and P. W. Fink, "An improved transformation and optimized sampling scheme for the numerical evaluation of singular and near-singular potentials," *IEEE Antennas Wireless Propagat. Lett.*, vol. 7, pp. 377–380, 2008.

[14] F. Vipiana, D. R. Wilton, W. A. Johnson, "Advanced Numerical Schemes for the Accurate Evaluation of 4-D Reaction Integrals in the Method of Moments," *IEEE Trans., Ant. and Propagat.*, vol. 61, 11, Nov. 2013, pp. 5559–5566.

[15] B. Eisenberg and R. Sullivan, "The Fundamental Theorem of Calculus in Two Dimensions," *Am. Math. Monthly*, vol. 109, 9., Nov. 2002, pp. 806–817.

[16] S. M. Rao, D. R. Wilton, and A. W. Glisson, "Electromagnetic scattering by surfaces of arbitrary shape," *IEEE Trans. Antennas Propag.*, vol. 30, 3, pp. 409–418, May 1982.

[17] A. H. Stroud, Approximate Calculation of Multiple Integrals, *Prentice-Hall*, NY, 1971.

[18] L. Zhang, T. Cui, and H. Liu, "A Set of Symmetric Quadrature Rules on Triangles and Tetrahedra," *J. Comp. Math.*, 27, 2009, pp. 89–96.

[19] P.C. Hammer, O.P. Marlowe and A. H. Stroud, "Numerical integration over simplexes and cones," in *Mathematical Tables and other Aids to Computation*, pp. 130–137, 1956.

[20] A. Gil, J. Segura, and N. Temme, "Chebyshev Expansions," in *Numerical Methods for Special Functions*, SIAM, 2007, ch. 3, pp. 51–86.

[21] J. Ma, V. Rokhlin, and S.Wandzura, "Generalized Gaussian quadrature rules for systems of arbitrary functions," *SIAM J. Numer. Anal.*, vol. 33, pp. 971–996, 1996.

[22] J. Ma, V. Rokhlin, and S. Wandzura, Generalized Gaussian Quadrature Rules for Systems of Arbitrary Functions, Tech. Rep. YALEU/DCS/RR-990, Oct. 1993, Dept. Computer Science, Yale University, New Haven, CT, USA.

[23] H. B. Dwight, Tables of Integrals and Other Mathematical Data, 4th Ed., *Macmillan*, NY, 1961.

APPENDIX A.

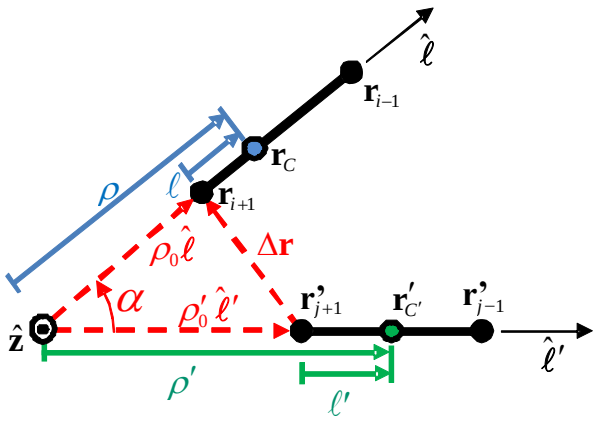

Figure 18. Geometry, global and local line segment parameterizations.

In Fig. 18, we assume we are given the line segment end point coordinates $\mathbf{r}_{i\pm1}, \mathbf{r}'_{j\pm1}$ of the test and source line segments, respectively, and we want to locate the intersection of their extensions. The two line segments shown in Fig. 18 are presumed to be the source triangle edge opposite vertex *j* and the test triangle edge opposite vertex *i*. (Only edges *i* and *j* of the source and test triangles are shown.) The quantities ρ, ρ' are segment arc lengths measured from the point of intersection of the extended line segments, while ℓ, ℓ' are local arc length parameterizations measured from endpoints of the source and test segments, respectively. The line segment unit vectors are $\hat{\ell}' = (\mathbf{r}'_{j-1} - \mathbf{r}'_{j+1})/|\mathbf{r}'_{j-1} - \mathbf{r}'_{j+1}|$ and $\hat{\ell} = (\mathbf{r}_{i-1} - \mathbf{r}_{i+1})/|\mathbf{r}_{i-1} - \mathbf{r}_{i+1}|$, and the two triangle outward normals (see Fig. 3) along the segments are $\hat{\mathbf{u}}' = \hat{\ell}' \times \hat{\mathbf{n}}$ and $\hat{\mathbf{u}} = \hat{\ell} \times \hat{\mathbf{n}}$. The angle between the line segments may be determined from $\cos\alpha = \hat{\ell}' \cdot \hat{\ell}$, $\sin\alpha = \hat{\mathbf{n}} \cdot (\hat{\ell}' \times \hat{\ell})$, and $\alpha = \tan^{-1}(\sin\alpha/\cos\alpha)$. (Use of the intrinsic function atan2, found in many programming languages, insures that α is placed in the proper quadrant of its range, $-\pi < \alpha \le \pi$.) Four separate cases may be identified:

- If $\hat{\mathbf{u}}' \cdot (\mathbf{r}'_{j+1} - \mathbf{r}_{i+1}) = \hat{\mathbf{u}}' \cdot (\mathbf{r}'_{j-1} - \mathbf{r}_{i-1}) = 0$ (or equivalently, if $\hat{\mathbf{u}} \cdot (\mathbf{r}'_{j+1} - \mathbf{r}_{i+1}) = \hat{\mathbf{u}} \cdot (\mathbf{r}'_{j-1} - \mathbf{r}_{i-1}) = 0$)) the segments are collinear and hence do not interact.
- If $|\sin\alpha| \le 10^{-6}$, $\cos\alpha > 0$, one should use (B.7) for $u(\rho, \rho')$; this case includes the parallel line segment limit $\alpha = 0$.
- If $|\sin\alpha| \le 10^{-6}$, $\cos\alpha < 0$, one should use (B.11) for $u(\rho, \rho')$; this case includes the anti-parallel line segment limit $\alpha = \pm\pi$. In both this and the previous case, we can assume that the point of intersection of the extended line segments always falls outside both line segments.
- If $|\sin\alpha| > 10^{-6}$, we first determine if the extended source segment intersects the test segment. From the figure, we note that $\rho_0\hat{\ell} - \rho_0'\hat{\ell}' = \mathbf{r}_{i+1} - \mathbf{r}'_{j+1} \equiv \Delta\mathbf{r}$. Dotting first with $\hat{\ell}$ and then with $-\hat{\ell}'$ yields the linear system

$$\begin{bmatrix} 1 & a' \\ a' & 1 \end{bmatrix} \begin{bmatrix} \rho_0 \\ \rho_0' \end{bmatrix} = \begin{bmatrix} c' \\ b' \end{bmatrix}, \tag{A.1}$$

written in matrix form and having the solution

$$\begin{bmatrix} \rho_0 \\ \rho_0' \end{bmatrix} = \frac{1}{1-a'^2} \begin{bmatrix} c' - a'b' \\ b' - a'c' \end{bmatrix}, \tag{A.2}$$

where

$$\begin{aligned} a' &= -\hat{\ell} \cdot \hat{\ell}', \; b' = -\Delta\mathbf{r} \cdot \hat{\ell}', \\ c' &= \Delta\mathbf{r} \cdot \hat{\ell}, \; d' = \Delta\mathbf{r} \cdot \Delta\mathbf{r}. \end{aligned} \tag{A.3}$$

If $-\Delta C < \rho_0 < 0$ the extended source segment intersects the test segment, the test segment must be subdivided at $\ell = |\rho_0|$, and the quadrature algorithm must then be applied to each subsegment separately. On the other hand, if $-\Delta C' < \rho_0' < 0$, the extended test segment intersects the source segment, the source segment must be subdivided at $\ell' = |\rho_0'|$, and the appropriate quadrature rule applied on each sub-segment.

In the above, $\Delta C'$ and ΔC are as depicted in Figs. 3 and 7 and defined following Eq. (11), and are the lengths of the source and test edges opposite vertices *j* and *i*, respectively. Also, the threshold $|\sin\alpha| \approx |\tan\alpha| = 10^{-6}$ above was found by testing a range of thresholds and determining that, for all ρ and ρ', below the threshold, the standard expression (38) for $u(\rho) = \tilde{u}(\rho, \rho')|_{\rho'=\rho'_L}^{\rho'_U}$ was not able to maintain double precision accuracy while the modified form of Appendix B was able to do so.

APPENDIX B.

From equation (35),

$$\begin{aligned} \frac{\partial\tilde{u}(\rho,\rho')}{\partial\rho} &= \rho\sin\alpha \; u'(\rho,\rho') \\ &= \sin\alpha \, h(\rho) R(\rho,\rho') + h^2(\rho)\cos\alpha \sinh^{-1}\left(\frac{\rho' - \rho\cos\alpha}{|h(\rho)|}\right). \end{aligned} \tag{B.1}$$

We define the first term on the right hand side of the second equality above as $u_1(\rho, \rho')$ and consider its integration as the indefinite integral

$$
\begin{aligned}
u_1(\rho,\rho') &= \sin^2\alpha\int \rho\, R(\rho,\rho')d\rho \\
&= \sin^2\alpha\int \rho\sqrt{\rho'^2+\rho^2-2\rho\rho'\cos\alpha}\,d\rho \\
&= \sin^2\alpha\frac{R^3(\rho,\rho')}{3}+\sin^2\alpha\frac{\rho'\cos\alpha(\rho-\rho'\cos\alpha)}{2}R(\rho,\rho') \\
&\quad+\frac{\rho'^3\cos\alpha\sin^4\alpha}{2}\int\frac{d\rho}{R(\rho,\rho')} \\
&= \sin^2\alpha\frac{R^3(\rho,\rho')}{3}+\sin^2\alpha\frac{\rho'\cos\alpha(\rho-\rho'\cos\alpha)}{2}R(\rho,\rho') \\
&\quad+\frac{\rho'^3\cos\alpha\sin^4\alpha}{2}\sinh^{-1}\left(\frac{\rho-\rho'\cos\alpha}{|h'(\rho')|}\right),
\end{aligned}
\tag{B.2}
$$

where Dw 380.211 and Dw 380.001 are used in the third and fourth equalities, respectively, with "Dw" referring to [23]. The remaining term, $u_2(\rho,\rho')$ in (B.1), may be integrated by parts, yielding

$$
\begin{aligned}
u_2(\rho,\rho') &= \cos\alpha\int\rho^2\sin^2\alpha\sinh^{-1}\left(\frac{\rho'-\rho\cos\alpha}{|\rho\sin\alpha|}\right)d\rho \\
&= \frac{\rho^3\sin^2\alpha\cos\alpha}{3}\sinh^{-1}\left(\frac{\rho'-\rho\cos\alpha}{|h(\rho)|}\right) \\
&\quad+\frac{\rho'\cos\alpha\sin^2\alpha}{3}\int\frac{\rho^2}{R(\rho,\rho')}\,d\rho.
\end{aligned}
\tag{B.3}
$$

The last integral in (B.3) is evaluated using Dw 380.021. and Dw 380. 001 as

$$
\begin{aligned}
&\int\frac{\rho^2}{R(\rho,\rho')}\,d\rho \\
&= \frac{(\rho+3\rho'\cos\alpha)R(\rho,\rho')}{2}+\frac{\rho'^2(3\cos^2\alpha-1)}{2}\int\frac{d\rho}{R(\rho,\rho')} \\
&= \frac{(\rho+3\rho'\cos\alpha)R(\rho,\rho')}{2} \\
&\quad+\frac{\rho'^2(3\cos^2\alpha-1)}{2}\sinh^{-1}\frac{\rho-\rho'\cos\alpha}{|h'(\rho')|}.
\end{aligned}
\tag{B.4}
$$

Combining (B.2), (B.3), (B.4) and simplifying, we obtain (38).

A. *Evaluation for small* $\tan\alpha$

The last two terms in (38) should be combined and evaluated as a Taylor series to prevent cancellation errors and to incorporate the limit when $\tan\alpha$ is small, i.e., when the source and test line segments are (anti-) parallel or nearly so. The last two terms of (38) can be written as

$$
\begin{aligned}
T &= \\
&= \frac{|h'|^3}{3\tan\alpha}\sinh^{-1}\left(\frac{\rho-\rho'\cos\alpha}{h'}\right)+\frac{|h|^3}{3\tan\alpha}\sinh^{-1}\left(\frac{\rho'-\rho\cos\alpha}{h}\right) \\
&= \frac{-\mathrm{sgn}(h)R^3}{3\tan\alpha}\Big[\mathrm{sgn}(h)\,\mathrm{sgn}(h')\cos^3(\theta'-\alpha)\,\sinh^{-1}\big(\tan(\theta'-\alpha)\big) \\
&\qquad-\cos^3\theta'\sinh^{-1}\big(\tan\theta'\big)\Big],
\end{aligned}
\tag{B.5}
$$

where in the last line, we have used (27), (28) and noted that

$$
\frac{\rho-\rho'\cos\alpha}{h'}=\tan\theta,\qquad \frac{\rho'-\rho\cos\alpha}{h}=\tan\theta'. \tag{B.6}
$$

Case α near 0:

Near $\alpha=0$, $\mathrm{sgn}(h)\,\mathrm{sgn}(h')=1$ and we can write T as

$$
T=-\mathrm{sgn}(h)\frac{R^3\cos\alpha}{3\left(\dfrac{\sin\alpha}{\alpha}\right)}\left(\frac{t(\alpha)-t(0)}{\alpha}\right), \tag{B.7}
$$

where $t(\alpha)=\cos^3(\theta'-\alpha)\,\sinh^{-1}\big(\tan(\theta'-\alpha)\big)$ and both factors in parentheses are bounded as $\alpha\to 0$. To calculate the factors accurately for small α, we replace each by its Maclaurin series approximation,

$$
\begin{aligned}
\frac{\sin\alpha}{\alpha} &= 1-\frac{\alpha^2}{6}+\frac{\alpha^4}{120}+\mathcal{O}(\alpha^6), \\
\frac{t(\alpha)-t(0)}{\alpha} &= t'(0)+\frac{t''(0)}{2}\alpha+\frac{t'''(0)}{6}\alpha^2+\mathcal{O}(\alpha^3),
\end{aligned}
\tag{B.8}
$$

where, noting that $d(\sinh^{-1}\tan x)/dx=1/|\cos x|$, terms on the right hand side of the second equality in (B.8) are found to be

$$
\begin{aligned}
t'(0) &= \cos^2\theta'\big[3\sin\theta'\sinh^{-1}(\tan\theta')-\mathrm{sgn}(\cos\theta')\big], \\
t''(0) &= (6\cos\theta'-9\cos^3\theta')\sinh^{-1}(\tan\theta')-5\big|\cos\theta'\big|\sin\theta' \\
t'''(0) &= \sin\theta'(6-27\cos^2\theta')\sinh^{-1}\big(\tan\theta'\big) \\
&\quad+(19\cos^2\theta'-11)\,\mathrm{sgn}(\cos\theta').
\end{aligned}
\tag{B.9}
$$

Case α near $\pm\pi$:

Near $\alpha=\pm\pi$, $\mathrm{sgn}(h)\,\mathrm{sgn}(h')=-1$. It is convenient to make the substitution $\alpha=(\mathrm{sgn}\,\alpha)\pi+\beta$, and to expand T about $\beta=0$, noting that

$$
\begin{aligned}
\cos(\theta'-\alpha) &= -\cos(\theta'-\beta), \\
\sin(\theta'-\alpha) &= -\sin(\theta'-\beta), \\
\tan(\theta'-\alpha) &= \tan(\theta'-\beta), \\
\tan\alpha &= \tan\beta.
\end{aligned}
\tag{B.10}
$$

This yields, finally

$$
T=-\mathrm{sgn}(h)\frac{R^3\cos\beta}{3\left(\dfrac{\sin\beta}{\beta}\right)}\left(\frac{t(\beta)-t(0)}{\beta}\right), \tag{B.11}
$$

where again we can use the Taylor series (B.8), (B.9) to approximate the quantities in parentheses.